

RESEARCH ARTICLE

Continuous and synchronous calibration process of ovality and straightness for longitudinally submerged arc welding pipes with three rollers

Xueying Huang^{1,2}*, Yubin Zhang²

1 Tianjin University, Ministry Education, Key Lab Mech Theory & Equipment Design, Tianjin, People's Republic of China, **2** School of Digital Technology and Engineering, Ningbo University of Finance and Economics, Ningbo City, People's Republic of China

* These authors contributed equally to this work.

* huangxueying@nbufe.edu.cn



OPEN ACCESS

Citation: Huang X, Zhang Y (2024) Continuous and synchronous calibration process of ovality and straightness for longitudinally submerged arc welding pipes with three rollers. PLoS ONE 19(8): e0307293. <https://doi.org/10.1371/journal.pone.0307293>

Editor: Rab Nawaz, COMSATS University Islamabad, PAKISTAN

Received: April 21, 2024

Accepted: July 3, 2024

Published: August 6, 2024

Copyright: © 2024 Huang, Zhang. This is an open access article distributed under the terms of the [Creative Commons Attribution License](https://creativecommons.org/licenses/by/4.0/), which permits unrestricted use, distribution, and reproduction in any medium, provided the original author and source are credited.

Data Availability Statement: All relevant data are within the paper and its [Supporting Information](#) files.

Funding: This project was funded and supported by General Project of Department of Education of Zhejiang Province [grant number Y202352463]. The funders had no role in study design, data collection and analysis, decision to publish, or preparation of the manuscript.

Competing interests: The authors have declared that no competing interests exist.

Abstract

A new process of continuous and synchronous calibration process of ovality and straightness for LSAW (Longitudinally Submerged Arc Welding, LSAW) pipes with three rollers is proposed. Specifically, the process is introduced from three aspects: roller-shape, loading parameters and axial and circumferential deformation paths. The process is verified by numerical simulation and physical experiments. Further, the stress-strain in the Sections II and IV is analyzed. The relationship between the process parameters and the residual ovality and residual straightness by experiments is discussed. The calibration scheme of LSAW pipes is put forward by using the control variable method. The results show that the shear stress is the principal stress direction in the Sections II and IV. The residual ovality and residual straightness decrease with the increase of the radial reduction and times of reciprocating bending. The reciprocating bending process can eliminate the difference of the initial curvature, make the curvature of each section tend to be uniform. After calibration, the residual straightness is less than 0.2% and the residual ovality is less than 1%, demonstrating a good feasibility of this process.

Introduction

With the development of the world's oil and gas resources transferring to unconventionality, remote and harsh development environment and the development trend of oversized transmission have put forward higher requirements for pipeline construction. Longitudinally Submerged Arc Welding (LSAW) pipes are made from high-steel wide plates, especially for long-distance oil and gas pipeline transportation and for laying pipes in deep-sea or cold areas. The ovality and straightness of the formed welded pipe cannot meet the industrial standards due to the factors such as welding thermal stress, material properties and technical equipment [1–3]. Therefore, the formed welded pipe needs to be rounded and straightened (the process of rounding and straightening is referred to as the calibration process in this paper). According

to the American Petroleum Institute's industry standard ANSI/API Spec. 5L, the ovality and straightness of finished welding pipes have been strictly required. The ovality of the finished welding pipe does not exceed $\pm 0.75\%$ of the nominal outer diameter, and the straightness is not greater than 0.2% of the total length of the pipe [4].

At present, the ovality calibration process mainly includes the whole-diameter ovality calibration process [5,6], the over-bending ovality calibration process [7–9], and the roll-type ovality calibration process [10–12]. Common straightness calibration techniques include the pressure straightening [13–15] and the cross-roll straightening [16–19]. The existing ovality and straightness calibration processes are done separately. On the one hand, it leads to the growth of production process and the reduction of production efficiency, which is not easy to realize automatic and intelligent production; On the other hand, because the deformation of ovality calibration and straightness calibration affect each other, the flattening problem of LSAW pipes cannot be solved [20]. It is difficult to adjust both the ovality and straightness to optimal levels, which also seriously affects on-site welding and pipeline safety [21]. In view of the application trend of LSAW pipes and the existing problem of ovality calibration technology and straightness calibration technology, a new three-roller continuous and synchronous calibration process of ovality and straightness is proposed. The new process is based on the principle of axial and circumferential bidirectional reciprocating bending, combining the ovality calibration process with the straightness calibration process [21–24].

The presence of high external pressure may cause buckling in the circular section of subsea pipelines. It can further lead to buckling propagation and even overall collapse [25]. Therefore, the rounding process is very crucial. The stress-strain distribution during the ovality calibration section is also a key factor. The residual stress in the pipe has a negative impact on the fatigue strength, stress corrosion resistance, service life and so on. If the residual stress distribution of the circumferential section of a pipe is not uniform, the ovality of the pipe will increase with the gradual release of the residual stress. As one of the most important processes before a pipe is put into production, it is necessary to study the stress and strain generated by the ovality calibration section [26–28].

Relevant scholars have studied the mechanical properties such as stress-strain and residual stress deeply. Yuhua et al. investigated welding cracks in micro laser-welded NiTiNb shape memory alloy and Ti6Al4V alloy dissimilar metals joints, providing valuable insights into the challenges of welding dissimilar metals, which is relevant to understanding the stress and deformation behaviors in welded structures [29]. Chen et al. discussed the effects of post-weld heat treatment on the microstructure and mechanical properties of laser-welded NiTi/304SS joints with Ni filler. It provided a broader understanding of the microstructural changes and mechanical property improvements possible with post-weld treatments [30]. Deng et al. presented a prediction model for the ultimate forming dimensions in the ring rolling process, which was pertinent to understanding deformation processes similar to those investigated in the calibration of LSAW pipes [31]. Hua et al. explored the mechanism of void healing in cold-rolled M50 bearing steel under electroshocking treatment through a combined experimental and simulation study. It contributed to the understanding of stress management and defect mitigation in metal processing [32]. Liu et al. provided a foundation for understanding the modeling techniques on mathematical modeling and analysis of the tailor-rolled blank manufacturing process that can be applied to similar deformation and calibration processes [33]. Zhu et al. presented an improved method for measuring welding residual stress, which was crucial for ensuring the structural integrity and performance of welded components, directly relevant to residual stresses in LSAW pipes [34]. Hu et al. provided insights into the fatigue behavior of high-entropy alloys, which was relevant for understanding material durability in LSAW pipes [35]. Zhang et al. discussed interface behavior and nanoindentation

characteristics in microbumps, offering comparative data on stress-strain behaviors [36]. Gao et al. explored elastic properties of auxetic structures, informing the deformation paths in LSAW pipes [37]. Wu et al. examined the impact of boron on structural stability in TLP joints, directly applicable to your calibration processes [38]. Additionally, Fang et al. provided valuable data on stress and strain behaviors during laser metal deposition, which could enhance the analysis of residual stresses [39]. Wang et al. and Liu et al. offered insights into mechanical performance and analytical methods [40,41]. Lastly, Long et al. presented findings on dynamic properties and predictive frameworks using machine learning, which could improve the analytical techniques in this research [42,43]. The above research has certain reference value for the understanding and study of the calibration process and mechanical properties of LSAW pipes in this paper.

The roller shapes, loading parameters, circumferential and axial deformation paths of the process are described in this paper. The distribution of stress-strain during the ovality calibration section is introduced by numerical simulation. The influencing factors of residual straightness and residual ovality are discussed. The feasibility of the process is verified by numerical simulation and physical experiments. The experimental platform is constructed and experiments are carried out. The calibration scheme for this process is proposed by using the control variable method.

Process introduction

The continuous and synchronous calibration process of ovality and straightness for LSAW pipes with three rollers is shown in Fig 1. The process' main working parts are three parallel rollers, including a convex roller (upper roller) and two concave rollers (lower rollers). The whole process is described as follows:

Depending on the size of the pipe, adjust the position of the three rollers so that the axes of each roller are parallel to each other. Then, push each roller with the same radial reduction toward the central axis of the pipe.

Two concave rollers rotate simultaneously driven by servo motors. This causes the pipe and convex roller to be driven to rotate under the action of friction. At the same time, the servo motor drives the push plate to make the pipe move along the slideway, thus enabling the calibration process.

Finally, the pipe is pushed out continuously until it is separated from three rollers. Each roller stops rotating this moment. The push plate moves automatically towards the opposite direction until it returns to its initial position, to complete the whole semi-automatic process.

Roller-shape

The schematic diagram of roller-shape is shown in Fig 2. Each roller is divided into five sections: loading section, ovality calibration section, ovality and straightness calibration section, ovality complement calibration section and unloading section.

As shown in Fig 2, both ends of the roller are loading section (Section I) and unloading section (Section V), both of which are truncated cone shape. The design enables the pipe to enter smoothly between the three rollers and ensures that the pipe can unload smoothly, so as to unify the curvature.

The taper of loading section and unloading section are respectively [23]

$$\alpha_j = \frac{3(2H_{\max} + 2a - D_p)}{L_g} \quad (1)$$

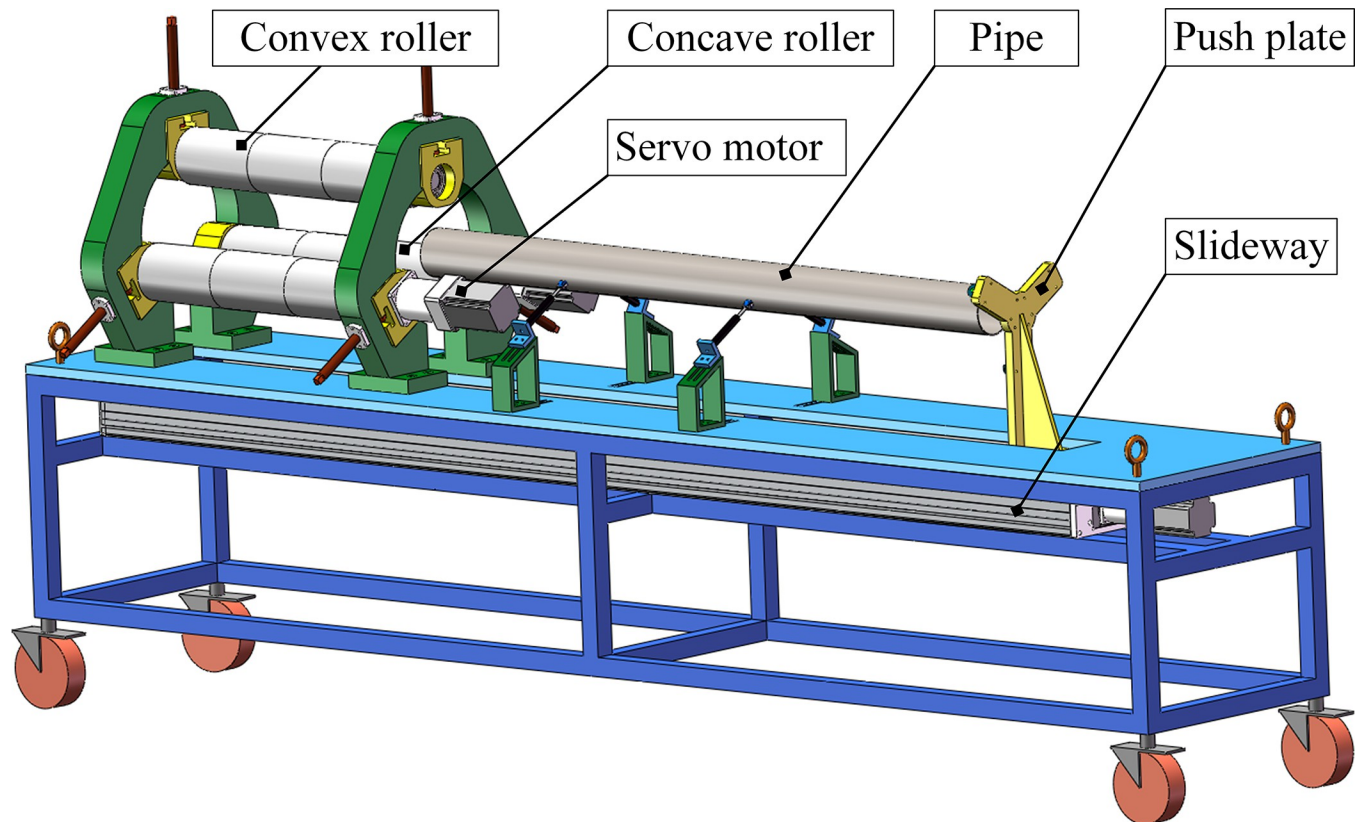


Fig 1. Schematic diagram of the calibration process.

<https://doi.org/10.1371/journal.pone.0307293.g001>

$$\alpha_x = \frac{6H_{\max}}{L_g} \quad (2)$$

Where α_j is the taper of loading section, α_x is the taper of unloading section, H_{\max} is the maximum radial reduction allowed for pipe calibrating, a is the major axis diameter of the pipe, D_p is the nominal outside diameter of the pipe, L_g is the length of roller.

Section II and Section IV are ovality calibration sections, which are cylindrical in shape. The design can make the pipe undergo multiple reciprocating bending along the circumferential direction, resulting in elastic-plastic deformation. Thus, ovality calibration and complementary ovality calibration are realized.

Section III is ovality and straightness calibration section. The upper roller part is convex and the lower roller part is concave. The design ensures that the pipe can undergo multiple reciprocating bending along the circumferential and axial directions. Thereby, ovality and straightness calibration are realized.

Loading parameter

Fig 3 is a schematic diagram of the loading parameter. The three rollers load the same radial reduction toward the pipe center, and the stroke of each roller is recorded as H .

$$H = R_1 + R - H_j \quad (3)$$

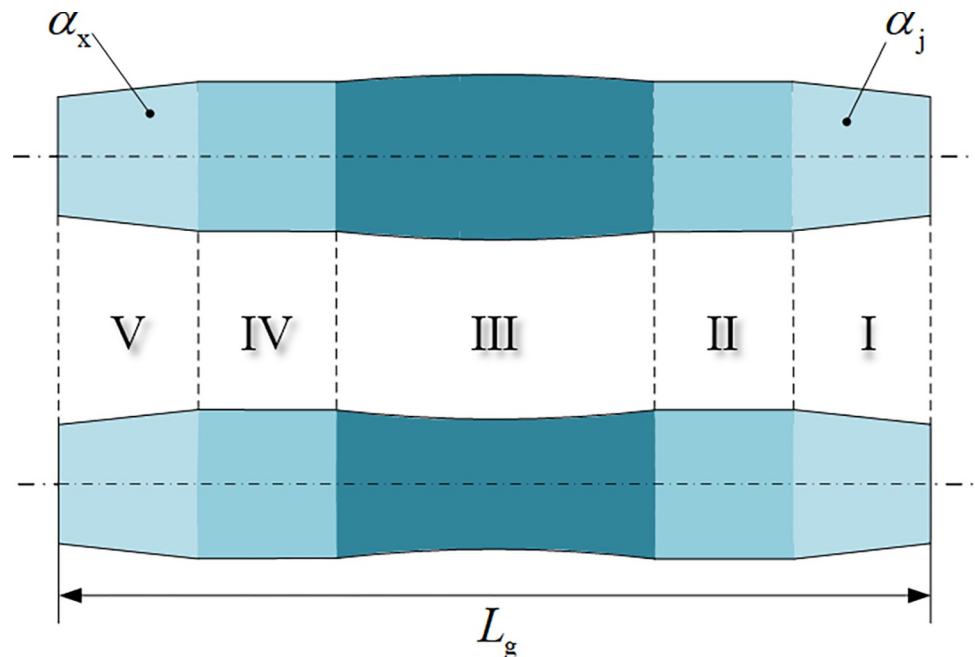


Fig 2. Schematic diagram of roller-shape. Section I: Loading section; Section II: Ovality calibration section; Section III: Ovality and straightness calibration section; Section IV: Ovality complement calibration section; Section V: Unloading section.

<https://doi.org/10.1371/journal.pone.0307293.g002>

where H is the radial reduction, R_1 is the roller radius, R is the pipe radius, H_j is the distance from the pipe's center to the center of roller after loading.

Deformation path of the axial reciprocating bending process

Since the pipe rotates and advances axially at the same time, any particle of the pipe alternately undergoes multiple positive-reverse bending process. The straightening process is an axial reciprocating bending process. The deformation path of the pipe particle along the axial direction is shown in Fig 4. The restraint and compression of the pipe by three rollers make it produce elastoplastic deformation within a certain range. To describe the reciprocating bending deformation process, any particle of the pipe is tracked. The trajectory of the particle Q is a spiral. Its center of rotation is the pipe axis. The deformation outside the plastic deformation zone is elastic deformation and has no influence on straightening.

As can be seen from Fig 4, particle Q reciprocates from position 1 to position 13. A total of 13 plastic bends is experienced throughout the straightening process. In the plastic deformation zone, the cross-sections at positions 2, 4, 6, 8, 10 and 12 are bent in a positive direction, and the cross-sections at positions 1, 3, 5, 7, 9, 11 and 13 are bent in a reverse direction. Since the Section III is a curve of variable curvature, the absolute value of curvature increases first and then decreases. That is, $|K_1| \rightarrow |K_2| \rightarrow |K_3| \rightarrow |K_4| \rightarrow |K_5| \rightarrow |K_6| \rightarrow |K_7|$ increases gradually, $|K_7| \rightarrow |K_8| \rightarrow |K_9| \rightarrow |K_{10}| \rightarrow |K_{11}| \rightarrow |K_{12}| \rightarrow |K_{13}|$ decreases gradually, and $K_1 = K_{13}$, $K_2 = K_{12}$, $K_3 = K_{11}$, \dots , $K_6 = K_8$.

Deformation path of the circumferential reciprocating bending process

Under the action of friction, the pipe does a rotational motion. Its circumferential cross-section alternately undergoes multiple positive bending process and reverse bending process. The

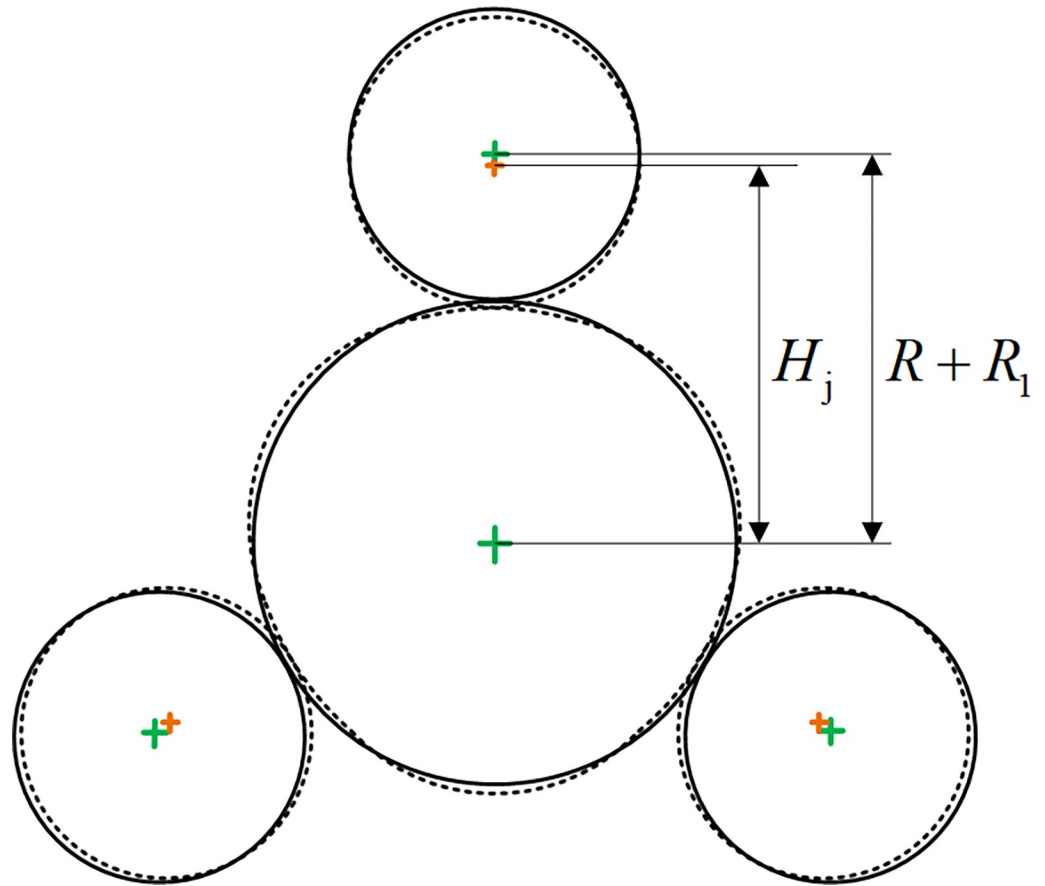


Fig 3. Diagram of loading parameters.

<https://doi.org/10.1371/journal.pone.0307293.g003>

pipe rounding process is a circumferential reciprocating bending process. Fig 5 shows the deformation trajectory of the pipe particle along the circumferential direction. The pipe is constrained and compressed by three rollers, resulting in elastoplastic deformation of the pipe in both positive and reverse bending zones. To describe the circumferential reciprocating bending deformation process, a section of the pipe-wall element of the pipe is selected.

With one rotation starting from position A, the continuous deformation process of the pipe-wall element is as follows:

1. The first positive bend: elastoplastic loading and unloading from position A to position B.
2. The first reverse bend: elastoplastic loading and unloading from position B to position C.
3. The second positive bend: elastoplastic loading and unloading from position C to position D.
4. The second reverse bend: elastoplastic loading and unloading from position D to position E.
5. The third positive bend: elastoplastic loading and unloading from position E to position F.
6. The third reverse bend: elastoplastic loading and unloading from position F to position A.

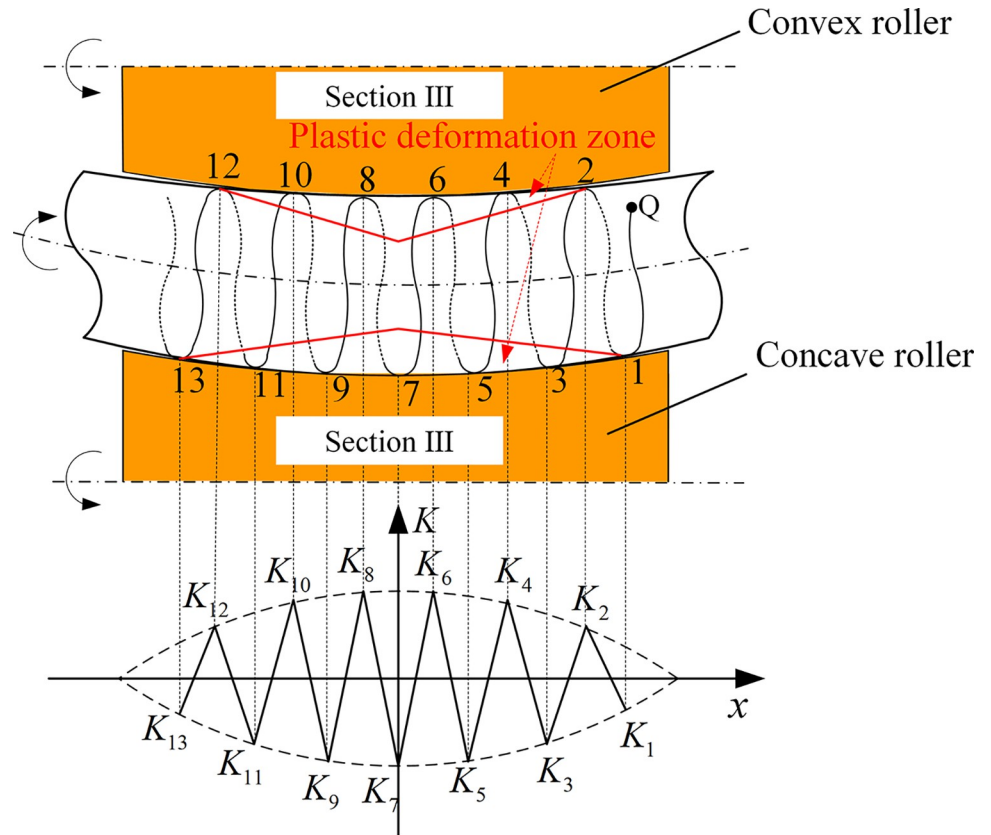


Fig 4. Deformation path of particle along axial direction.

<https://doi.org/10.1371/journal.pone.0307293.g004>

Numerical simulation and experimental design

The flow chart for formulating the calibration scheme by numerical simulations and physical experiments is shown in Fig 6. As mentioned above, radial reduction and times of reciprocating bending are the main process parameters. To determine the times of reciprocating bending, it is necessary to solve the ratio of roller rotation speed (V_r) to pipe forward speed (V_f). (Fig 6) The ratio is discussed based on numerical simulation analyses. Then, the times of reciprocating bending is obtained. Based on the control variable method, the influence of process parameters on the residual ovality and residual straightness is obtained through experiments. Combining the above analysis results, a solution is proposed, that is, the calibration scheme of the process.

The number of reciprocating bending is calculated from the beginning of contact with three rollers to completely leaving three rollers. The number of reciprocating bending cycles was determined through the roller rotation speed (V_r) and the pipe forward speed (V_f). The equation to be solved is as follows,

$$\psi = \frac{L_p V_r}{\pi D_p V_f} \tag{4}$$

Where, ψ is the number of reciprocating bending; V_r is the roller rotation speed (mm/s); V_f is the pipe forward speed (mm/s); L_p is the pipe length (mm); D_p is the pipe outer diameter (mm).

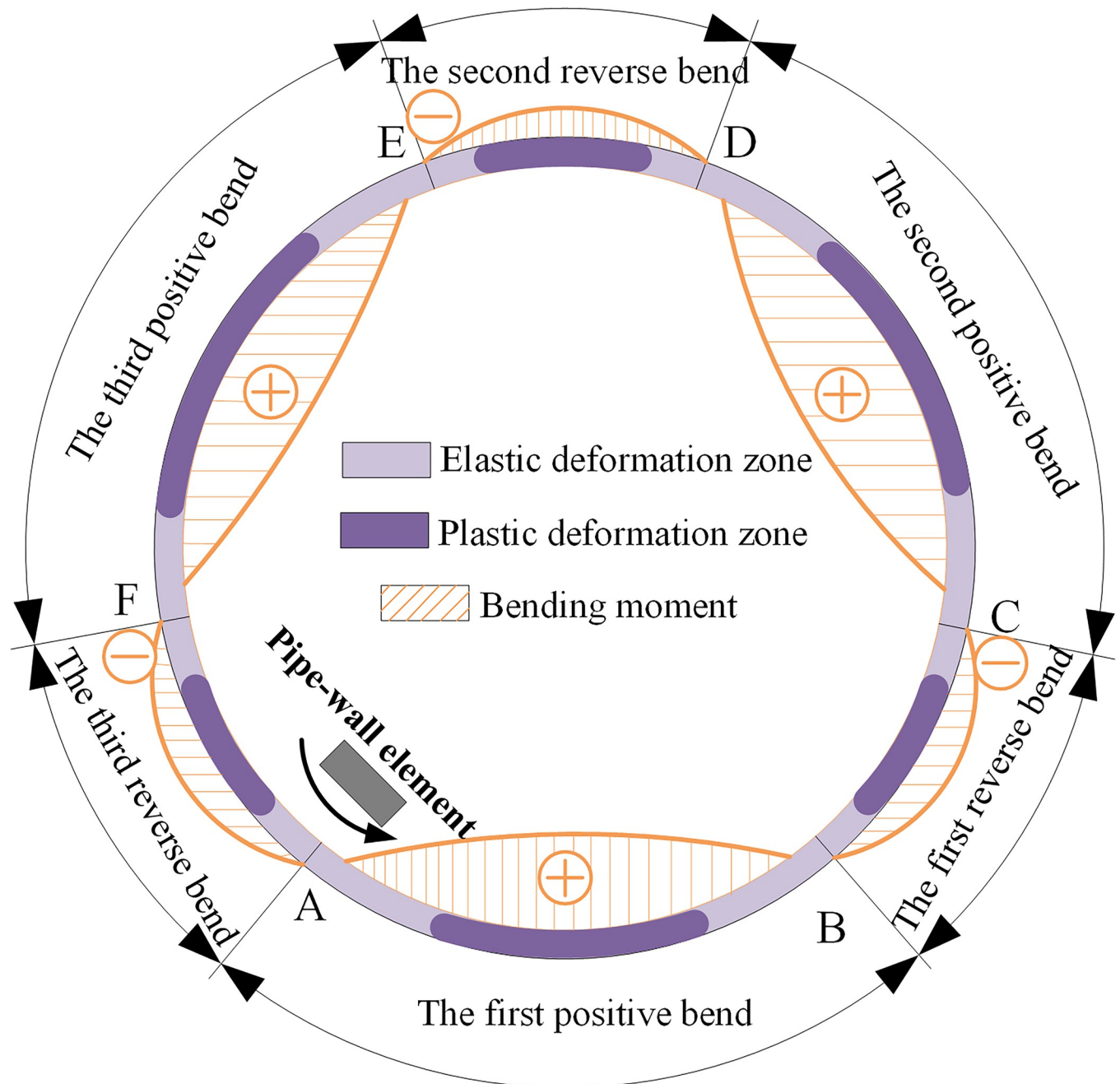


Fig 5. Deformation path of particle along circumferential direction.

<https://doi.org/10.1371/journal.pone.0307293.g005>

Numerical simulation

Using the software ABAQUS, a finite element model of the LSAW pipe calibration process is established, as shown in Fig 7. Regardless of the pipe welds on the continuous calibration process, the mechanical properties and geometric dimensions of pipes are shown in Table 1 and the geometric dimensions of rollers is shown in Table 2. The pipe is set as a deformable body. The pipe-wall is divided into 4 layers along the thickness. The pipe is discretized by 8-node linear hexagonal nonconforming mode elements. Select the continuum distributing coupling method to couple the center point of the pipe and the boundary. Six degrees of freedom for the

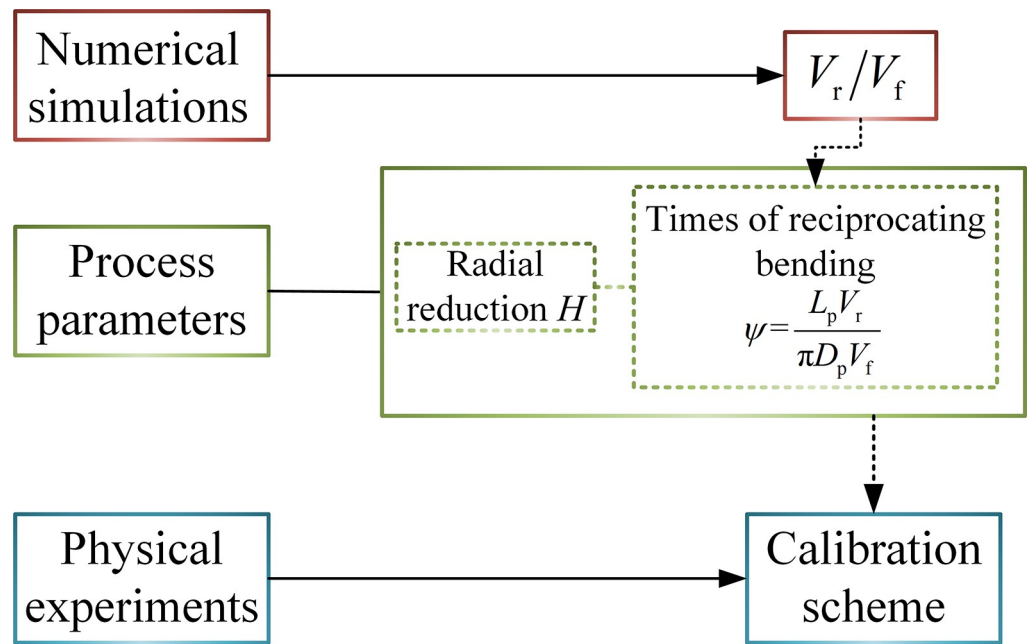


Fig 6. Flow chart for formulating the calibration scheme.

<https://doi.org/10.1371/journal.pone.0307293.g006>

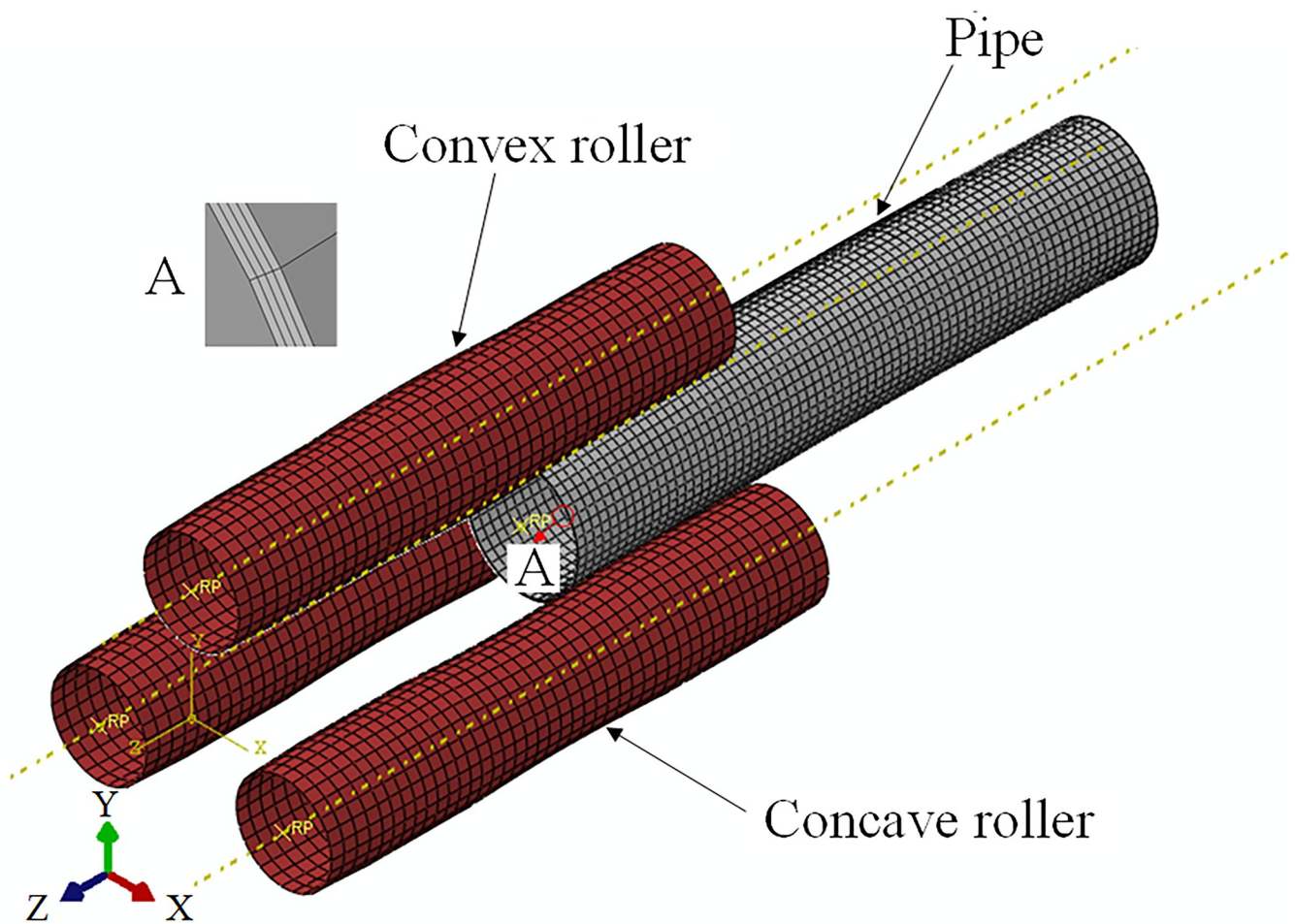


Fig 7. Finite element model.

<https://doi.org/10.1371/journal.pone.0307293.g007>

Table 1. Mechanical properties and geometric dimensions of pipes.

Material	Elastic modulus E (GPa)	Yield stress σ_s (MPa)	Plastic modulus D (MPa)	Outer diameter D_p (mm)	Length L_p (mm)	Thickness t (mm)	Initial ovality	Initial straightness
304	234	294	2842	140/160	1000	2/1.5	5%	10‰

<https://doi.org/10.1371/journal.pone.0307293.t001>

Table 2. Geometric dimension of rollers.

Outer diameter D_g (mm)	Length L_g (mm)	Proportion of rollers	Taper of Section I (rad)	Taper of Section V (rad)	K_n (mm^{-1})	Roller shape curve of Section III
120	600	1:2:4:2:1	0.033	0.025	0.001	$0.16x^2 - 0.0004y^2 - 1 = 0$

<https://doi.org/10.1371/journal.pone.0307293.t002>

constrained area is selected. The three rollers are set as discrete rigid bodies. The contact between the pipe and each roller is set to pure master-slave contact and motion contact conditions. The coefficient of friction is 0.2.

Experimental design

The experimental device for pipe calibration is shown in Fig 8. The device can realize both continuous rounding and continuous straightening of LSAW pipes.

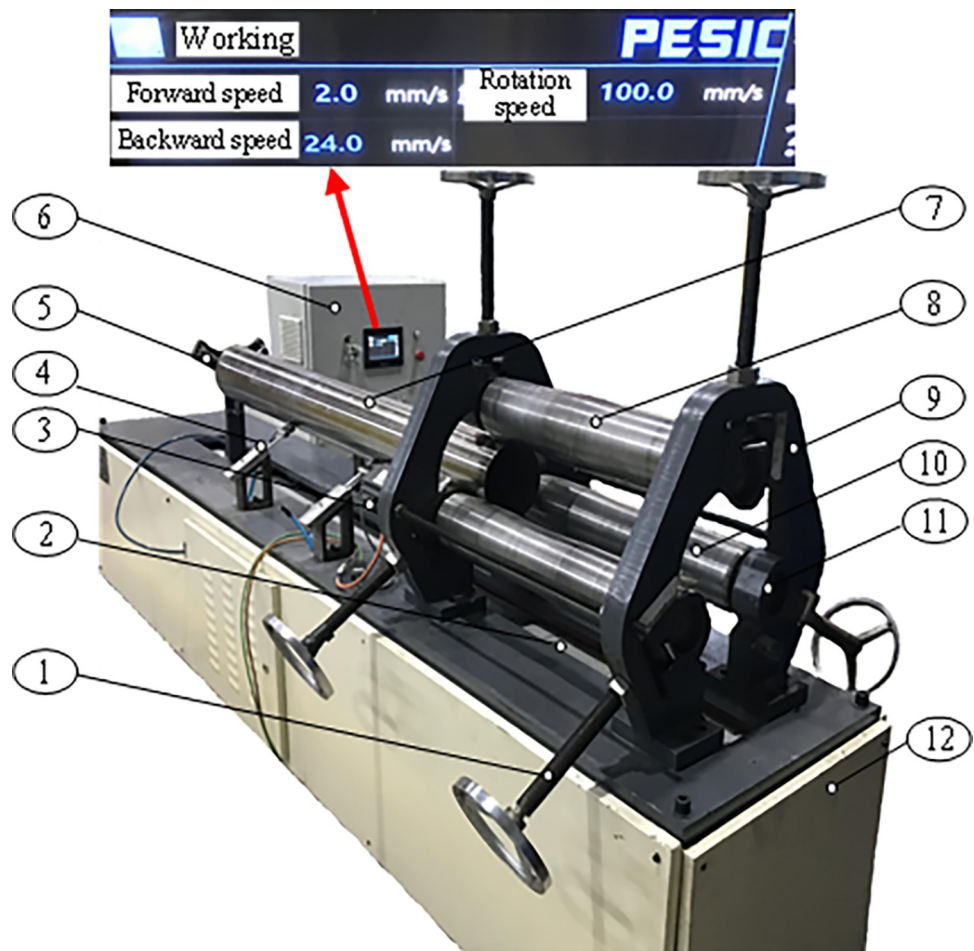


Fig 8. Experimental device for pipe calibration. 1. Screw 2. Lead screw drive 3. Servo motor 4. Support assembly 5. Push plate 6. Control cabinet 7. Pipe 8. Upper roller 9. Frame 10. Lower roller 11. Slider 12. Pedestal.

<https://doi.org/10.1371/journal.pone.0307293.g008>

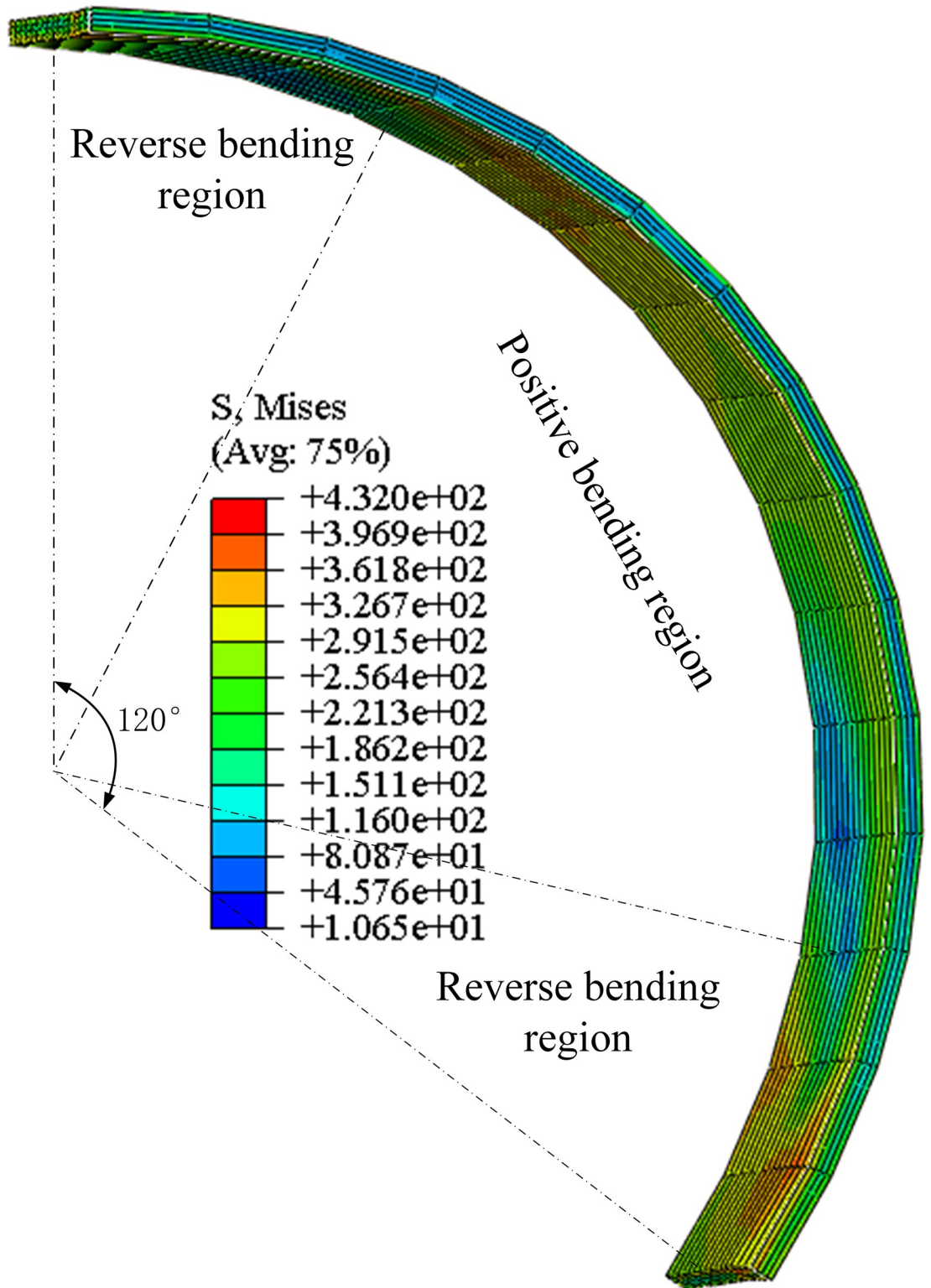


Fig 9. Distribution of equivalent stress along the one-third pipe.

<https://doi.org/10.1371/journal.pone.0307293.g009>

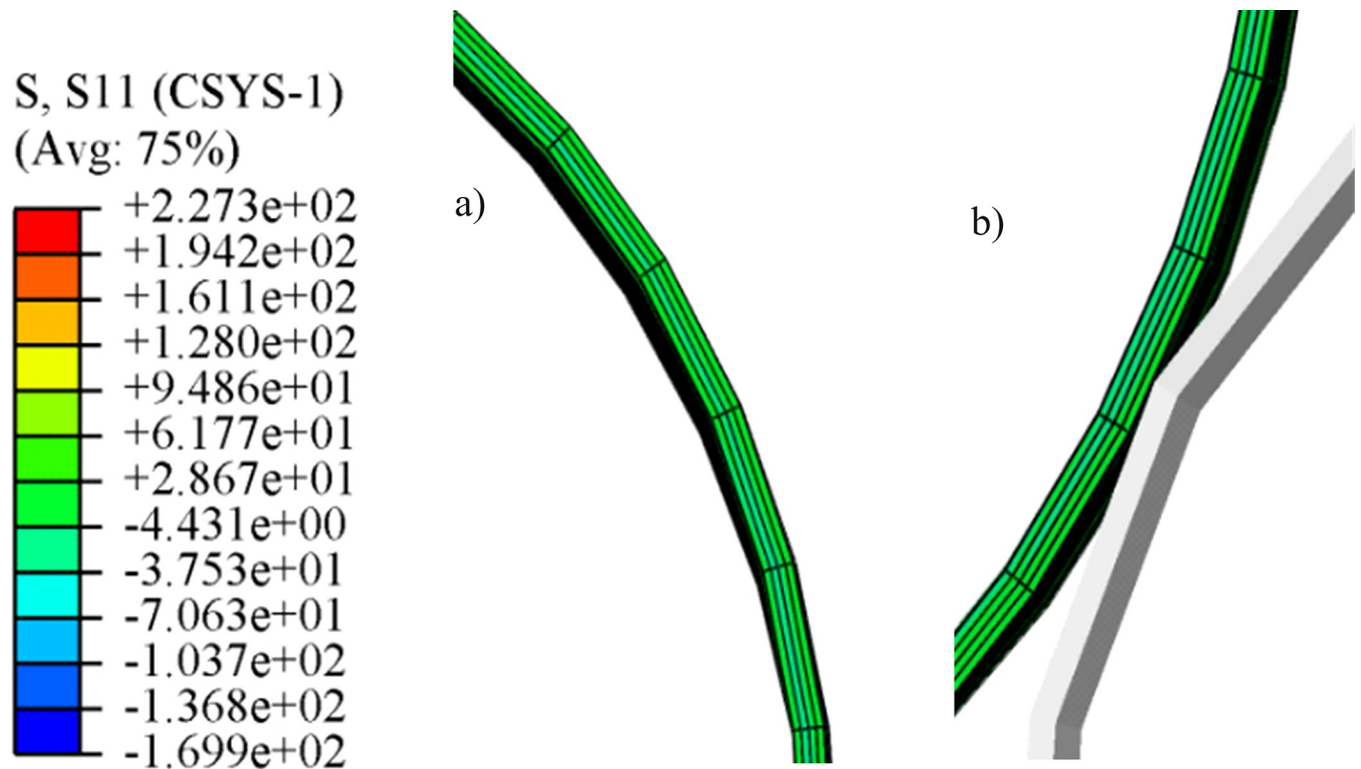


Fig 10. Distribution of radial stress along the thickness direction. a) Positive bending region; b) Reserve bending region.

<https://doi.org/10.1371/journal.pone.0307293.g010>

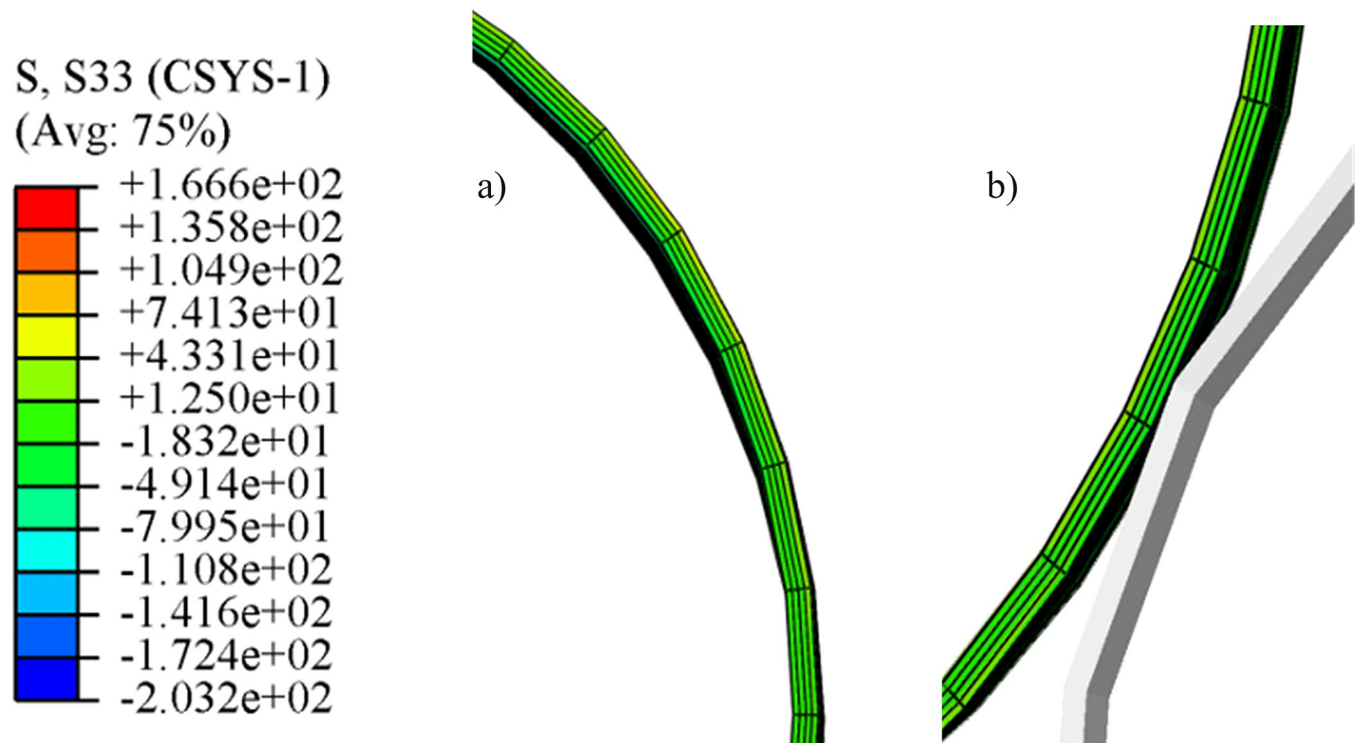


Fig 11. Distribution of axial stress along the thickness direction. a) Positive bending region; b) Reserve bending region.

<https://doi.org/10.1371/journal.pone.0307293.g011>

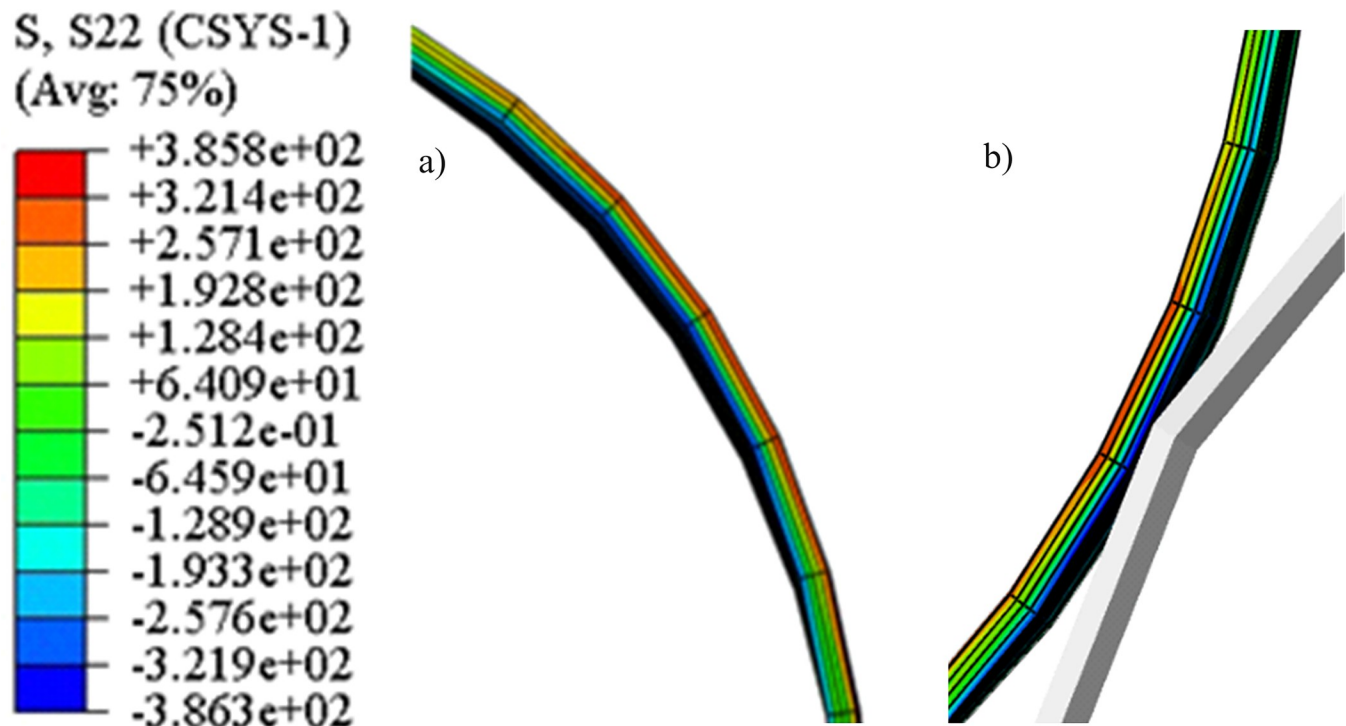


Fig 12. Distribution of shear stress along the thickness direction. a) Positive bending region; b) Reserve bending region.

<https://doi.org/10.1371/journal.pone.0307293.g012>

The roller is connected with the slider fixed on the frame via bearing (Fig 8). The slider can slide vertically along the frame surface via a screw to adjust the radial reduction of three rollers. The support assembly keeps the balance of the pipe during the experiment. The servo motor drives two lower rollers to rotate synchronously, which drives the pipe and the upper roller to start turning. At the same time, the push plate drives the pipe to move along the sideway. So far, the calibration process of simultaneous rotation and movement of the pipe is realized. The pipes and rollers selected for the experiment are the same as the pipes and rollers selected for the simulation.

Results and discussion

Simulation results

Ovality calibration section (Sections II and IV). The equivalent stress distribution along the one-third pipe is shown in Fig 9. According to the symmetry of the circle, there are three positive bending regions and three reverse bending regions.

The distribution of radial stress along the thickness direction is shown in Fig 10. The radial stress of the pipe is small and does not reach the yield stress of the material. So, it does not produce elastoplastic deformation. Therefore, it can be assumed that the geometric dimensions along the thickness of the pipe do not change during the ovality calibration section.

The distribution of axial stress along the thickness direction is shown in Fig 11. The deformation behavior of the inner and outer material fibers of the pipe is inhibited. The axial stress of the pipe is very small and will not cause plastic deformation. During the ovality calibration section, the geometry does not change along the length of the pipe.

The distribution of shear stress along the thickness direction is shown in Fig 12. In the positive bending region, the maximum stress value of the outer fiber is 321.4MPa, and the

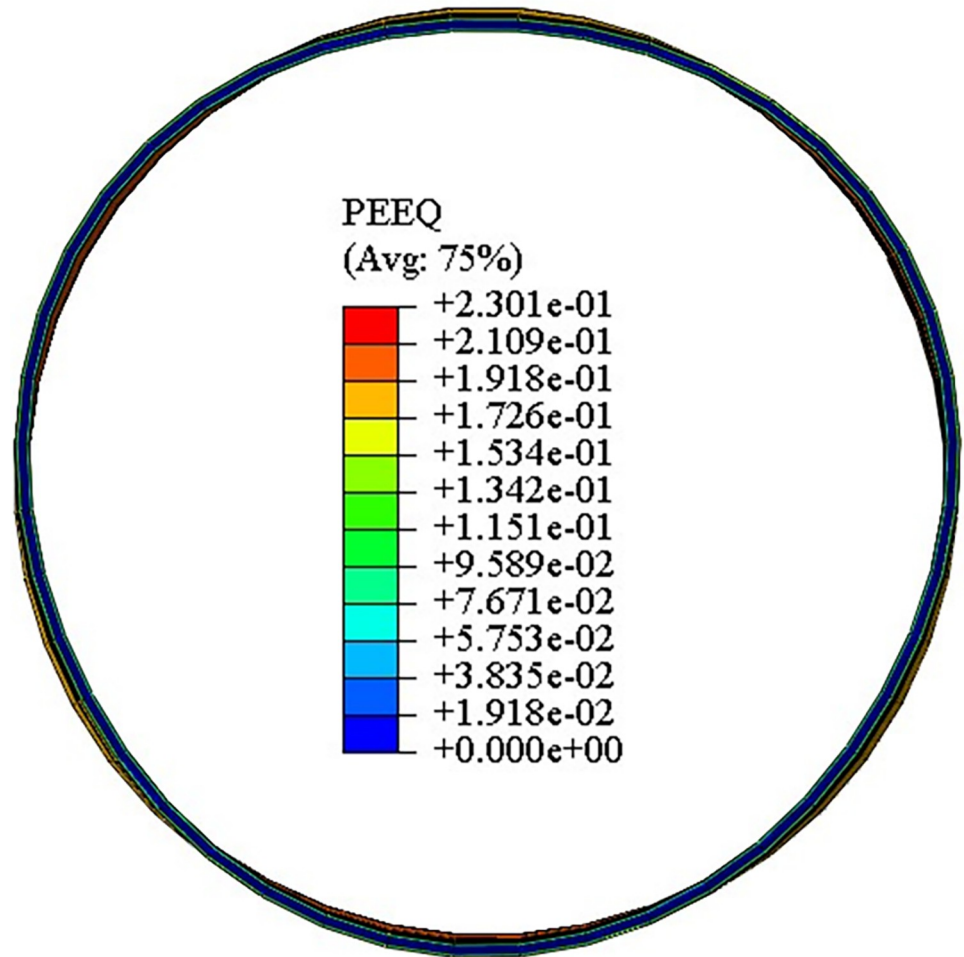


Fig 13. Distribution of equivalent strain in the ovality calibration section.

<https://doi.org/10.1371/journal.pone.0307293.g013>

minimum stress value of the inner fiber is -321.9MPa. In the reverse bending region, the minimum stress value of the outer fiber is -386.3MPa, and the maximum stress value of the inner fiber is 385.8MPa. The shear stress causes the inner and outer layers of the pipe to enter the yield stage first, resulting in plastic deformation. Therefore, the direction in which the shear stress is located is the main stress direction.

The distribution of equivalent strain in the ovality calibration section is shown in Fig 13. The deformation behavior of the pipe belongs to the small deformation. Its equivalent strain value is also small. The maximum equivalent strain value is 0.23 in the main deformation region and 0 in the geometrically neutral layer.

The equivalent stress distribution of 304 pipe after calibration is shown in Fig 14. The distribution of equivalent stress tends to be uniform and the residual stress is small.

Determination of key parameters. As can be seen from reference [12], the larger the diameter-thickness ratio of the pipe, the less likely it is to achieve calibration. To reduce the simulation times, the pipe with large diameter-thickness ratio is selected for analysis. In this paper, the pipe with a diameter of 160 mm and a thickness of 1.5 mm is selected as the research object. The ratio of roller rotation speed (V_r) to pipe forward speed (V_f) is determined by numerical simulation. The effect of the ratio of V_r to V_f on residual ovality and residual straightness is shown in Fig 15.

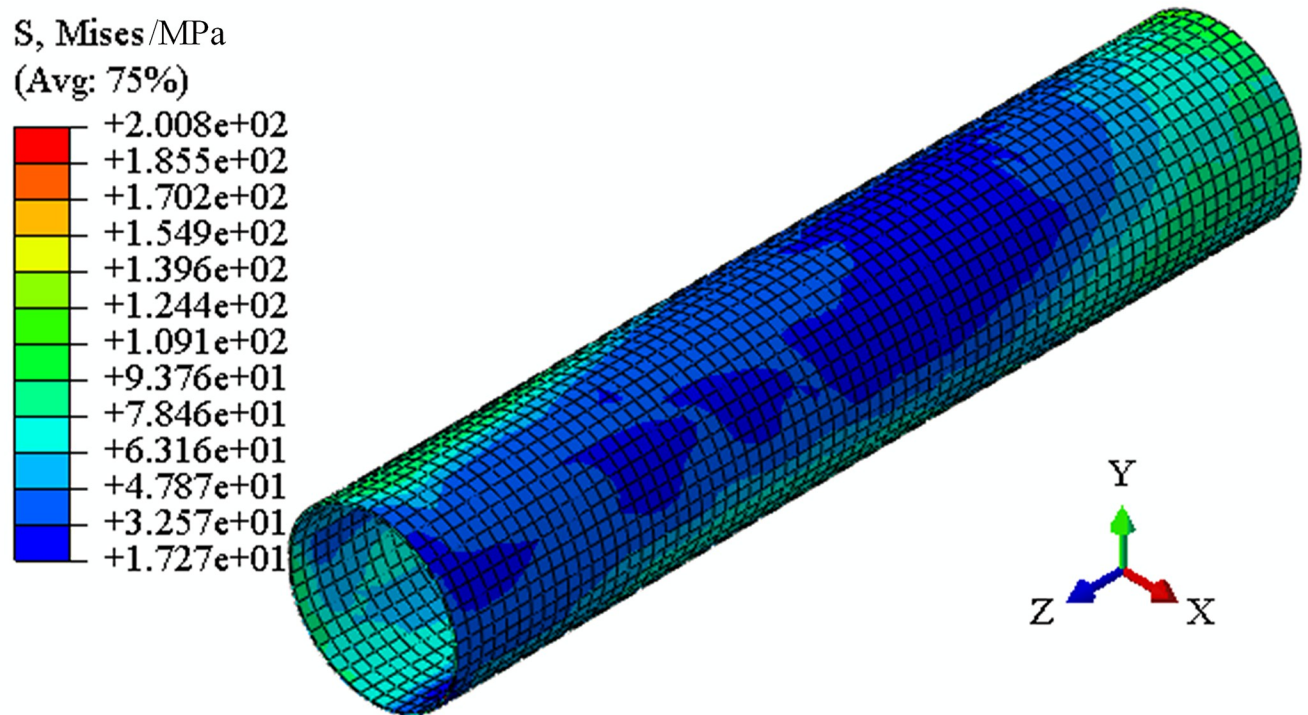


Fig 14. Distribution of residual stress of 304 pipe after calibration.

<https://doi.org/10.1371/journal.pone.0307293.g014>

The residual ovality and residual straightness of the pipe gradually decrease with the increase of the ratio of V_r to V_f . When $V_r/V_f \geq 25$, the residual ovality is within 1% and the residual straightness is within 2‰. The results meet the standard requirements [4]. As a result, the feasibility of the process is initially verified. It should be noted that the ratio should not be less than 25 in the experiment.

Experimental results. According to the above simulation results, the ratio of V_r to V_f has been determined. When the the ratio of V_r to V_f is 25, the radial reduction (H) of pipes is discussed. The pipes with a diameter of 160 mm with a thickness of 1.5 mm, 2.0 mm and 2.5mm are selected as the research object. The effect of radial reduction on residual ovality and residual straightness of pipes is shown in Fig 16. It can be observed that the residual ovality and residual straightness gradually decrease with the increase of radial reduction. Fig 16A shows that the residual ovality of the pipe is within 1% when $H > 1.5$ mm. Fig 16B shows that the residual straightness of the pipe is within 0.2‰ when $H > 1.7$ mm. In conclusion, the residual ovality and residual straightness of the above pipes meet the industry standards [4].

According to the simulation results, the times of reciprocating bending ψ on the residual ovality and residual straightness of pipes is discussed when the H is 1.5 mm and 1.7 mm. The ratio of V_r to V_f is 20, 25, 30, 35, 40, 45, the number of reciprocating bends is 40, 50, 60, 70, 80, and 90, respectively. The effect of the times of reciprocating bending on residual ovality and residual straightness of pipes is shown in Fig 17.

The residual ovality and residual straightness of pipes gradually decrease with the increase of the times of reciprocating bending. When the times of reciprocating bending is not less than 50, the residual ovality of pipes is within 1% and the residual straightness is within 0.2‰. The above results lay the foundation for the development of subsequent calibration schemes.

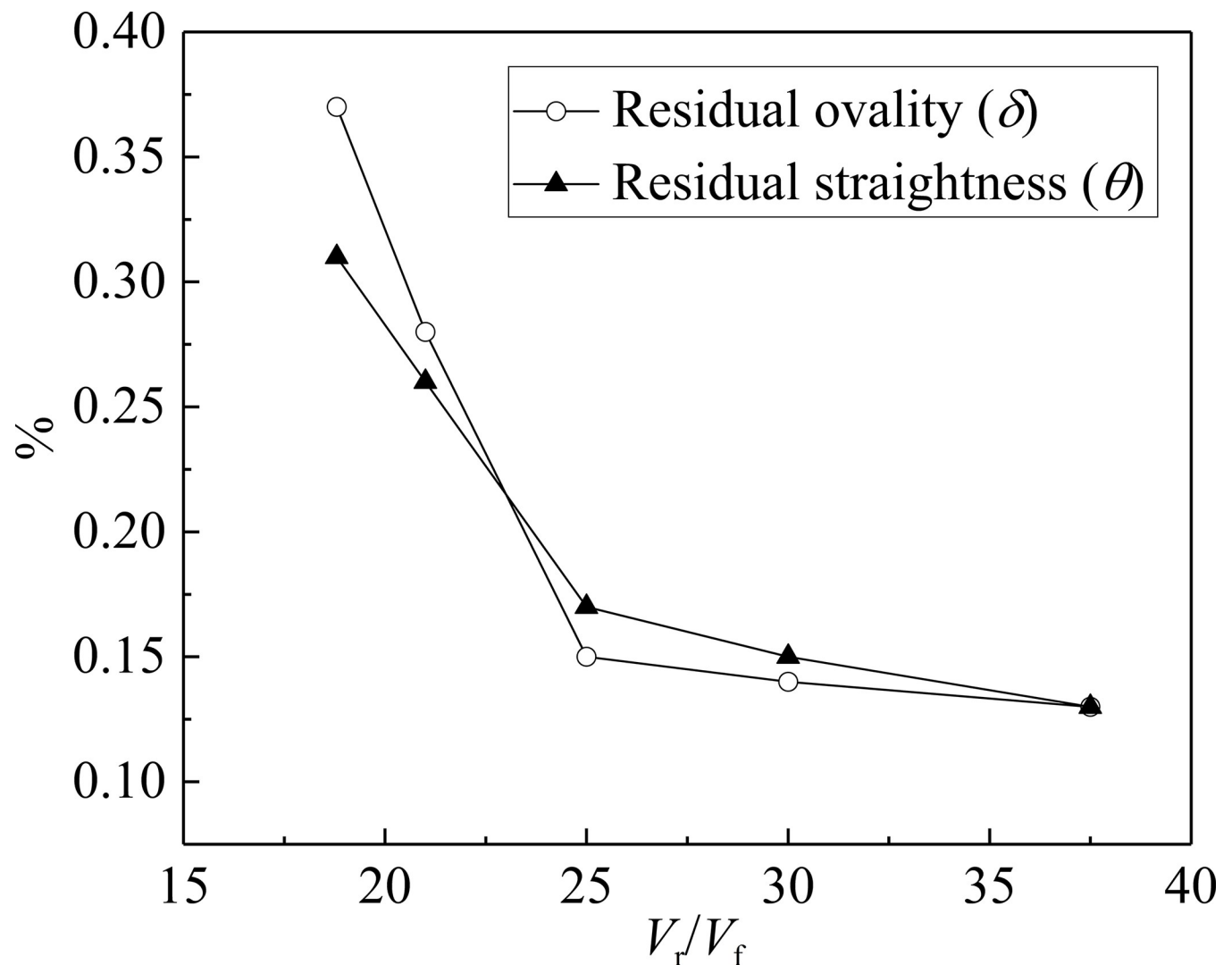


Fig 15. Effect of the ratio of V_r to V_f on residual ovality and residual straightness.

<https://doi.org/10.1371/journal.pone.0307293.g015>

After calibration, the residual ovality and residual straightness can meet the industry standards [4]. The forming effect of 304 stainless steel pipes is shown in Fig 18.

Calibration scheme

As discussed earlier, a calibration scheme is proposed by considering process parameters, experimental device, roller-shape, material, and geometric dimension of pipes. It should be noted that the radial reduction, roller rotation speed and pipe forward speed are the direct input parameters of the experiment. It is therefore necessary to determine the above. The calibration scheme is as follows:

1. Loading parameter (radial reduction H): For pipes with a diameter of 160 mm with a thickness of 1.5 mm, 2.0 mm and 2.5mm, calibration is available when the radial reduction is 1.7 mm.
2. The ratio of roller rotation speed (V_r) to pipe forward speed (V_f): The ratio of V_r to V_f is related to the times of reciprocating bending and the geometric dimension (length and

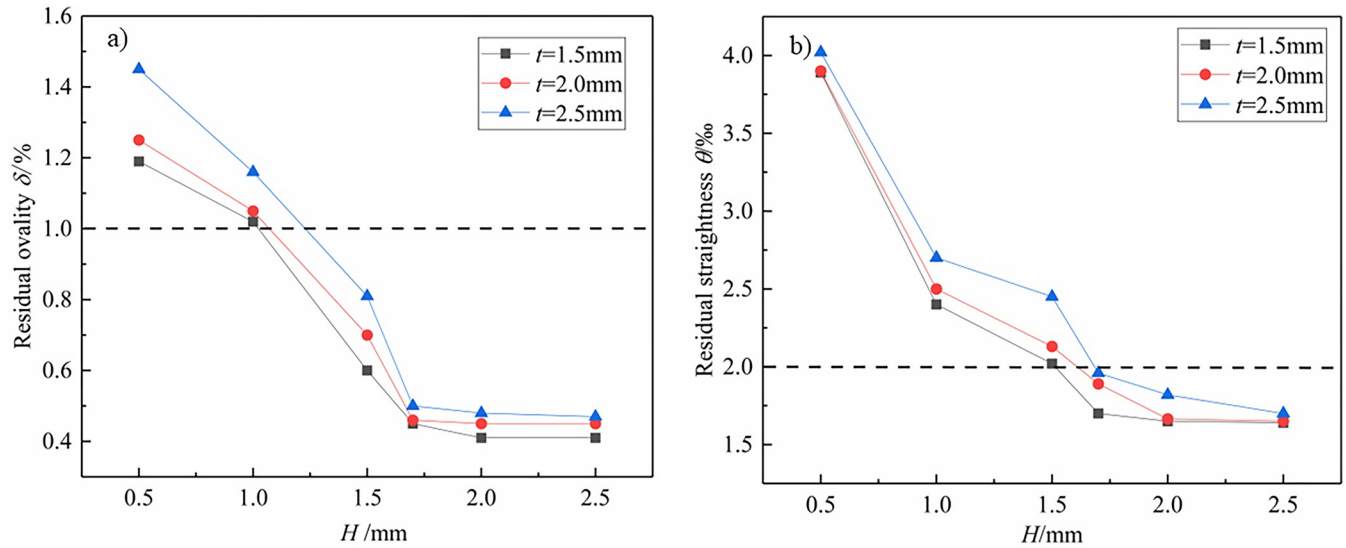


Fig 16. Effect of radial reduction on residual ovality and residual straightness of pipes. a) Residual ovality; b) Residual straightness; the times of reciprocating bending ψ is 50.

<https://doi.org/10.1371/journal.pone.0307293.g016>

outer diameter) of pipes. Experimental results show that the residual ovality and residual straightness of pipes can meet the industry standard when the times of reciprocating bending is not less than 50. So the ratio of V_r to V_f can be calculated in the case of known pipe's size and the times of reciprocating bending. According to the ratio, V_r and V_f can be reasonably assigned within the controlled range of the experimental device operating system.

Conclusions

1. A new process of continuous and synchronous calibration process of ovality and straightness for LSAW pipes with three rollers is proposed. An experimental device is developed,

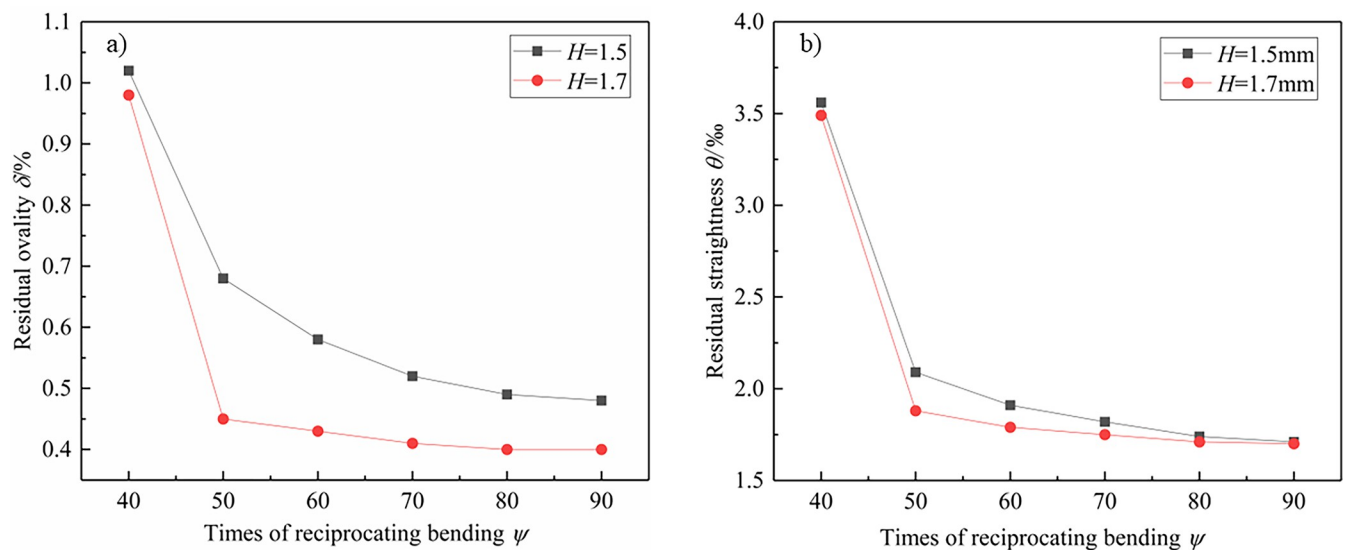


Fig 17. Effect of the times of reciprocating bending on residual ovality and residual straightness of pipes. a) Residual ovality; b) Residual straightness; $t = 2.0\text{mm}$.

<https://doi.org/10.1371/journal.pone.0307293.g017>

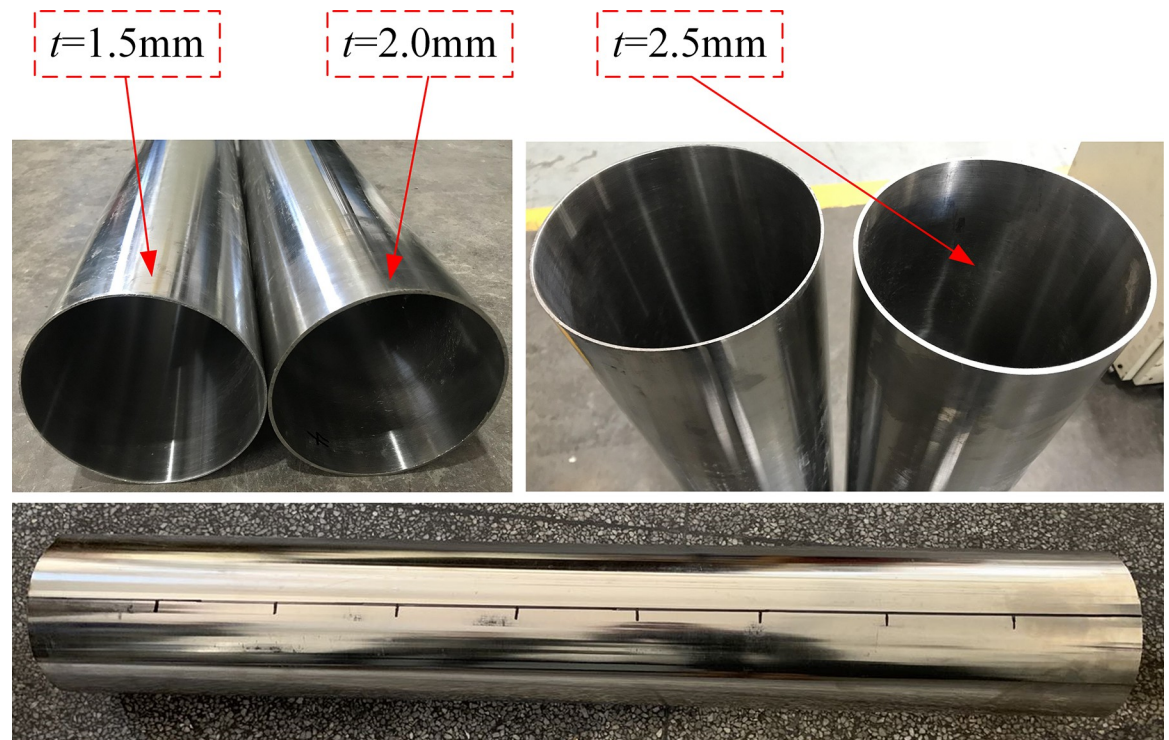


Fig 18. Forming effect of 304 stainless steel pipes.

<https://doi.org/10.1371/journal.pone.0307293.g018>

which can realize the two functions of continuous calibrating ovality and continuous calibrating straightness of LSAW pipes.

2. Through the analysis of shear stress, radial stress, and axial stress, it is concluded that the shear stress is the main stress direction. Three positive bending regions and three reverse bending regions are distributed uniformly along the circumferential direction of the pipe.
3. The influence of process parameters on residual ovality and residual straightness is discussed. That is, the residual ovality and residual straightness of pipes decrease with the increase of the radial reduction and times of reciprocating bending. The reciprocating bending process can eliminate the difference of initial curvature and unify the circumferential and axial curvature to the same direction and value respectively.
4. A calibration scheme based on the process is proposed by using the control variable method. In view of the calibration scheme, the radial reduction, roller rotation speed and pipe forward speed can be determined. It provides guidance for the application of the process in practical production. The residual ovality of pipes is within 1% and the residual straightness is within 0.2%, which complies with the requirements of API standard.

Supporting information

S1 File.
(DOCX)

Author Contributions

Conceptualization: Xueying Huang.

Data curation: Xueying Huang.

Formal analysis: Xueying Huang.

Funding acquisition: Xueying Huang.

Investigation: Xueying Huang.

Methodology: Xueying Huang.

Project administration: Xueying Huang.

Resources: Xueying Huang.

Software: Xueying Huang, Yubin Zhang.

Supervision: Xueying Huang.

Validation: Xueying Huang.

Visualization: Xueying Huang, Yubin Zhang.

Writing – original draft: Xueying Huang.

Writing – review & editing: Xueying Huang.

References

1. Deng D, Murakawa H, Liang W (2008) Numerical and experimental investigations on welding residual stress in multi-pass butt-welded austenitic stainless-steel pipe. *Computational Materials Science* 42(2): 234–244. <https://doi.org/10.1016/j.commatsci.2007.07.009>
2. Law M, Prask H, Luzin V, Gnaeupel-Herold T (2006) Residual stress measurements in coil linepipe and girth welded pipe. *Materials Science and Engineering A* 437(1): 60–63. <https://doi.org/10.1016/j.msea.2006.04.062>
3. Yaghi A, Hyde TH, Becker AA, Sun W, Williams JA (2008) Residual stress simulation in thin and thick-walled stainless steel pipe welds including pipe diameter effects. *International Journal of Pressure Vessels and Piping* 83(11–12): 864–874. <https://doi.org/10.1016/j.ijpvp.2006.08.014>
4. ANSI/API Specification 5L, Specification for line pipe (forty-fifth edition). Washington DC, United States, 2012.
5. Yin J, Zhao J, Qu XY, Zhai RX (2011) Springback analysis of expanding and setting round for large diameter pipe. *Journal of Mechanical Engineering* 47(12): 32–42. <https://doi.org/10.3901/JME.2011.12.032>
6. Yin J, Zhao J, Sun HL, Zhan PP (2011) Precise compression and setting round by mould for large pipes. *Optics and Precision Engineering* 19(9): 2072–2078. <https://doi.org/10.3788/OPE.20111909.2072>
7. Zhao J, Zhan PP, Ma R, Zhai RX (2012) Control strategy of over-bending setting round for pipe-end of large pipes by mould press type method. *Transactions of Nonferrous Metals Society of China* 22(S2): 329–334. [https://doi.org/10.1016/S1003-6326\(12\)61727-0](https://doi.org/10.1016/S1003-6326(12)61727-0)
8. Zhao J, Zhan PP, Ma R, Zhai RX (2013) Quantitative prediction of reduction in large pipe setting round process. *Chinese Journal of Mechanical Engineering (English Edition)* 26(4): 722–729.
9. Zhao J, Zhan PP, Ma R, Zhai RX (2014) Prediction and control of springback in setting round process for pipe-end of large pipe. *International Journal of Pressure Vessels and Piping* 116(1): 56–64. <https://doi.org/10.1016/j.ijpvp.2014.01.006>
10. Yu GC, Zhao J, Zhai RX, Ma R, Wang CG (2018) Theoretical analysis and experimental investigations on the symmetrical three-roller setting round process. *International Journal of Advanced Manufacturing Technology* 94(12): 45–56. <https://doi.org/10.1007/s00170-016-9610-4>
11. Zhao J, Yu GC, Ma R (2016) A mechanical model of symmetrical three-roller setting round process: The static bending stage. *Journal of Materials Processing Technology* 231: 501–512. <https://doi.org/10.1016/j.jmatprotec.2016.01.002>

12. Yu GC, Zhao J, Xing JJ, Zhao FP, Li SL (2017) Research on the symmetrical three-roller setting round process. *Journal of Mechanical Engineering* 53(14): 136–143. <https://doi.org/10.3901/JME.2017.14.136>
13. Zhao J, Song XK (2014) Control strategy of multi-point bending one-off straightening process for LSAW pipes. *International Journal of Advanced Manufacturing Technology* 72(9–12): 1615–1624. <https://doi.org/10.1007/s00170-014-5776-9>
14. Zhao J, Song XK, Cao HQ, Liu J (2014) Press straightening control strategy of multi-step three-point bending for LSAW pipes. *Journal of Harbin Institute of Technology* 46(1): 90–96. <https://doi.org/10.11918/j.issn.0367-6234.2014.01.016>
15. Zhao J, Song XK, Cao HQ, Liu J (2014) Principle of multi-point bending one-off straightening process for longitudinally submerged arc welding pipes. *Journal of Mechanical Engineering* 50(2): 92–97. <https://doi.org/10.3901/JME.2014.02.092>
16. Yu GC, Zhai RX, Zhao J, Ma R (2018) Theoretical analysis and numerical simulation on the process mechanism of two-roller straightening, *International Journal of Advanced Manufacturing Technology* 94(9): 4011–4021. <https://doi.org/10.1007/s00170-017-1120-5>
17. Liu ZJ, Ma LD, Li JH, Du YK, Meng ZJ (2020) Accuracy analysis of six skewed-roll straightening process of tube. *Journal of Iron and Steel Research* 32(9): 55–61. <https://doi.org/10.13228/j.boyuan.issn1001-0963.20200014>
18. Wang CG, Yu GC, Wang W, Zhao J (2018) Deflection detection and curve fitting in three-roll continuous straightening process for LSAW pipes. *Journal of Materials Processing Technology* 255: 150–160. <https://doi.org/10.1016/j.jmatprotec.2017.11.060>
19. Wang CG, Zhang ZY, Zhai RX, Yu GC, Zhao J (2018) Cross-sectional distortion of LSAW pipes in over-bend straightening process. *Thin-Walled Structures* 129(AUG.): 85–93. <https://doi.org/10.1016/j.tws.2018.03.016>
20. Cui F, Yang HL (2015) New understanding in the field of straightening theory. *Heavy Machinery* 2–5. <https://doi.org/10.3969/j.issn.1001-196X.2015.01.001>
21. Huang XY, Yu GC, Zhai RX, Ma R, Zhou C, Gao CL, Zhao J (2021) Roller design and numerical simulation of three-roller continuous and synchronous adjusting straightness and ovality process on LSAW pipes. *Journal of Mechanical Engineering* 57(10): 148–159. <https://doi.org/10.3901/JME.2021.10.148>
22. Huang XY, Yu GC, Zhao J, Mu ZK, Zhang ZY, Ma R (2020) Numerical simulation and experimental investigations on a three-roller setting round process for thin-walled pipes. *International Journal of Advanced Manufacturing Technology* 107: 355–369. <https://doi.org/10.1007/s00170-020-05087-2>
23. Huang XY, Zhao J, Yu GC, Meng QD, Zhai RX (2021) Three-roller continuous setting round process for longitudinally submerged arc welding pipes. *Transactions of Nonferrous Metals Society of China* 31(5): 1411–1426. [https://doi.org/10.1016/S1003-6326\(21\)65586-3](https://doi.org/10.1016/S1003-6326(21)65586-3)
24. Zhao J, Yu GC, WANG HR (2017) A roller-type continuous and synchronous calibrating straightness and ovality equipment and processing method for pipes. Hebei: CN106623507A, 2017-05-10.
25. Xie P, Chang JT, Chen XB (2023) Study on the crushing bearing capacity of submarine pipelines with ellipticity and corrosion defects. *Journal of Ship Mechanics* 27(07): 1096–1108.
26. Yang JH (2023) Study on residual stress of three-roll continuous rounding process for large thin-walled tube. Yanshan University. <https://doi.org/10.27440/d.cnki.gysdu.2023.000813>
27. Huang XY, Yu GC, Wang CG, Zhao J (2022) Deformation mechanism analysis of three-roller continuous and synchronous calibration process of straightness and roundness for LSAW pipes. *International Journal of Advanced Manufacturing Technology* 121(3): 1731–1742. <https://doi.org/10.1007/s00170-022-09426-3>
28. Huang XY, Gu JP (2024) A theoretical model for roller-shape design of three-roller continuous and synchronous calibration process of ovality and straightness for large thin-walled pipes. *Sci Rep* 14, 7094. <https://doi.org/10.1038/s41598-024-57753-0> PMID: 38528082
29. Chen YH, Mao YQ, Lu WW, He P. Investigation of welding crack in micro laser welded NiTiNb shape memory alloy and Ti6Al4V alloy dissimilar metals joints. *Optics & Laser Technology*. 2017, 91, 197–202. <https://doi.org/10.1016/j.optlastec.2016.12.028>.
30. Chen Y, Sun S, Zhang T, Zhou X & Li S. Effects of post-weld heat treatment on the microstructure and mechanical properties of laser-welded NiTi/304SS joint with Ni filler. *Materials Science and Engineering: A*. 2020, 771, 138545. <https://doi.org/10.1016/j.msea.2019.138545>.
31. Deng J, Wu R, Sun Z, Qian D & Zhang Y. A prediction model of ultimate forming dimension for profile ring with outer groove in ring rolling process. *The International Journal of Advanced Manufacturing Technology*. 2024, 130(1), 491–510. <https://doi.org/10.1007/s00170-023-12528-1>

32. Hua L, Liu Y, Qian D, Xie L, Wang F, Wu M. Mechanism of void healing in cold rolled aeroengine M50 bearing steel under electroshocking treatment: A combined experimental and simulation study. *Materials Characterization*. 2020, 185, 111736. <https://doi.org/10.1016/j.matchar.2022.111736>.
33. Liu Y, Wang T, Wang Z & Huang Q. Mathematical modeling and analysis of the tailor rolled blank manufacturing process. *International Journal of Mechanical Sciences*. 2024, 266, 108991. <https://doi.org/10.1016/j.ijmecsci.2024.108991>.
34. Zhu Q, Chen J, Gou G, Chen H & Li P. Ameliorated longitudinal critically refracted—Attenuation velocity method for welding residual stress measurement. *Journal of Materials Processing Technology*. 2017, 246, 267–275. <https://doi.org/10.1016/j.jmatprotec.2017.03.022>.
35. Hu J, Yang K, Wang Q, Zhao QC, Jiang YH, Liu YJ. Ultra-long life fatigue behavior of a high-entropy alloy. *International Journal of Fatigue*. 2024, 178, 108013. <https://doi.org/10.1016/j.ijfatigue.2023.108013>
36. Zhang Z, Chen J, Wang J, Han Y, Yu Z, Wang Q, Zhang P, Yang S. Effects of solder thickness on interface behavior and nanoindentation characteristics in Cu/Sn/Cu microbumps. *Welding in the World*. 2022, 66 (5): 973–983. <https://doi.org/10.1007/s40194-022-01261-0>
37. Gao Q, Ding Z, Liao WH. Effective elastic properties of irregular auxetic structures. *Composite Structures*. 2022, 287, 115269. <https://doi.org/10.1016/j.compstruct.2022.115269>
38. Wu Y, Chen J, Zhang L, Ji J, Wang Q, Zhang S. Effect of boron on the structural stability, mechanical properties, and electronic structures of γ' -Ni₃Al in TLP joints of nickel-based single-crystal alloys. *Materials Today Communications*. 2022, 31, 103375. <https://doi.org/10.1016/j.mtcomm.2022.103375>
39. Fang JX, Ma GZ, Tian HL, Li SB, Huang HS, Liu Y, et al. Transformation-induced strain of a low transformation temperature alloy with high hardness during laser metal deposition. *Journal of Manufacturing Processes*. 2021, 68: 1585–1595. <https://doi.org/10.1016/j.jmapro.2021.06.066>
40. Wang S, Chen X, Luo K, Zhou H, Li R, He P, et al. The design of low-temperature solder alloys and the comparison of mechanical performance of solder joints on ENIG and ENEPIG interface. *Journal of Materials Research and Technology*. 2023, 27: 5332–5339. <https://doi.org/10.1016/j.jmrt.2023.11.066>
41. Liu J, Xu J, Paik KW, He P, Zhang S. In-situ isothermal aging TEM analysis of a micro Cu/ENIG/Sn solder joint for flexible interconnects. *Journal of Materials Science and Technology*. 2024, 169: 42–52. <https://doi.org/10.1016/j.jmst.2023.06.020>
42. Long X, Su T, Lu C, Wang S, Huang J, Chang C. An insight into dynamic properties of SAC305 lead-free solder under high strain rates and high temperatures. *International Journal of Impact Engineering*. 2023, 175, 104542. <https://doi.org/10.1016/j.ijimpeng.2023.104542>
43. Long X, Lu C, Su Y, Dai Y. Machine learning framework for predicting the low cycle fatigue life of lead-free solders. *Engineering Failure Analysis*. 2023, 148, 107228. <https://doi.org/10.1016/j.engfailanal.2023.107228>